Available online at www.sciencedirect.com

ScienceDirect

Procedia Engineering 190 (2017) 464 – 471

Procedia Engineering

www.elsevier.com/locate/procedia

Structural and Physical Aspects of Construction Engineering

FEM Modelling of Lateral-Torsional Buckling using Shell and Solid Elements

Jan Valeš[a,*], Tudor-Cristian Stan[b]

[a]*Brno University of Technology, Faculty of Civil Engineering, Department of Structural Mechanics, Veveří St. 95, ZIP 602 00, Brno, Czech Republic*

[b]*Technical University of Denmark, Department of Civil Engineering, Brovej 118, 2800 Kgs. Lyngby, Denmark*

Abstract

The paper describes two methods of FEM modelling of I-section beams loaded by bending moments. Series of random realizations with initial imperfections following the first eigenmode of lateral-torsional buckling were created. Two independent FEM software products were used for analyses of resistance. At the end the difference and correlation between the results as well as advantages and disadvantages of both methods are discussed.

Peer-review under responsibility of the organizing committee of SPACE 2016

Keywords: Imperfection; Beam; Steel; Lateral-torsional buckling; FE modelling; Stability

1. Introduction

The aim of the paper is to carry out a stochastic analysis of load-carrying capacity of steel beams subjected to bending. A series of simply supported IPE200 beams are analyzed with respect to lateral-torsional buckling, which is a stability phenomenon that occurs when an unrestrained member is subjected to moment loads. The analysis is carried out by using geometrically and materially nonlinear imperfect analyses (GMNIA) so the effects of all initial imperfections can be taken into account.

Two ways of modelling and carrying out the analysis of load-carrying capacity were chosen at both universities, the Czech one and the Danish one, respectively. The paper also compares the results from both working places and

* Corresponding author. Tel.: +420 541 147 116; fax: +420 541 240 994.
E-mail address: vales.j@fce.vutbr.cz

Peer-review under responsibility of the organizing committee of SPACE 2016
doi:10.1016/j.proeng.2017.05.365

point out to the advantages and disadvantages of both approaches. The first and the second method use shell model in Abaqus software and solid model in Ansys software, respectively. Therefore, the model differences concern boundary conditions and ways of loading as well. Material model, residual stress distribution and initial geometrical imperfections are considered the same in both cases.

The analyses are performed for three values of non-dimensional slenderness: 0.3, 0.6 and 1.2. Initial random material characteristics and cross-section dimensions were generated using the Latin Hypercube Sampling method and they were identical for each slenderness. The geometrical imperfection has been $e_0 = L/1000$, a choice based on recommendations from [1] and practice used in developing the Eurocode buckling curves [2].

2. Computational model description

FE research was carried out for models of steel beams of the European double symmetric hot-rolled profile IPE200. Beams are simply supported with fork-end boundary conditions and they are loaded by bending moments M on both ends. This represents a case of pure bending.

2.1. Initial geometrical imperfection

The initial out-of-straightness imperfection is designed according to the first eigenmode of buckling. Thus, the initial imperfect shape includes as out-of-plane displacement v_0 as torsional imperfection φ_0, see Fig. 1.

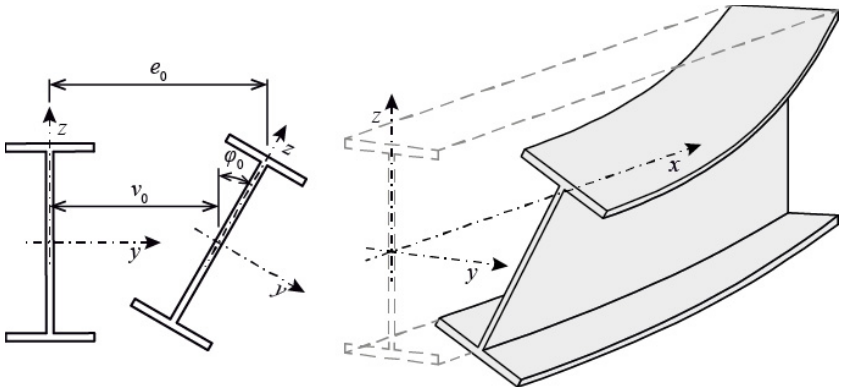

Fig. 1. initial out-of-straightness imperfection.

These imperfections are assumed to be affine to the deformed shape and to be shaped in sine wave form:

$$v_0 = a_{v0} \sin\left(\frac{\pi x}{L}\right), \ \varphi_0 = a_{\varphi_0} \sin\left(\frac{\pi x}{L}\right), \tag{1}$$

where a_{v0} and $a_{\varphi 0}$ are amplitudes given as

$$a_{v0} = \frac{e_0}{1 + \frac{h}{2}\frac{\pi^2 EI_z}{M_{cr}L^2}}, \ a_{\varphi_0} = a_{v_0}\frac{\pi^2 EI_z}{M_{cr}L^2}, \tag{2}$$

where e_0 is the amplitude of deformation at mid-span, L is the span-length of the beam, h is the cross-section height, I_z is the second moment of area to the axis z, E is the Young's modulus of elasticity and M_{cr} is the elastic critical moment at lateral beam buckling, see e.g. [3].

The size of geometrical imperfection is $e_0 = L/1000$. That implies that all beams of the same length and thus the same slenderness have the same geometrical imperfections. Even though it does not reflect real beams adequately, it is sufficient for this type of study.

2.2. Non-dimensional slenderness

Three different values of non-dimensional slenderness according to [4] are considered in this analysis: $\overline{\lambda}_{LT} \in (0.3,0.6,1.2)$. Table 1 shows the relation between non-dimensional slenderness and length considering nominal material characteristics and cross-section dimensions.

Table 1. Non-dimensional slenderness and beam length.

Slenderness	Length
0.3	0.73 m
0.6	1.55 m
1.2	3.86 m

2.3. Abaqus model

The commercial software program ABAQUS [5] has been used for the finite element analyses using shell elements at the Danish university. The beams are modelled using the general purpose S4 shell element (with full integration). This element has 4 corner nodes with 6 degrees of freedom and is applicable for analysis involving finite membrane strains and large rotations. 16 elements per flange width, 16 elements per web height and 200 elements per beam length are used in order to obtain accurate results and approximate a linear distribution of residual stresses.

The *x*-axis corresponds to the longitudinal beam axis and the *y*-axis and *z*-axes are in the plane of the cross section. The *y*-axis is parallel to the web and the *z*-axis is parallel to the flanges. The origin of the (*y*; *z*) axes is situated at the elastic center of the cross section. The nodal displacements are referred to as the displacements (U_x; U_y; U_z) and the rotations (R_x; R_y; R_z) respectively in and about the global coordinate directions (*x*; *y*; *z*), see Fig. 2. The end support conditions are modelled using kinematic coupling constraints, which relate the displacement of a group of nodes to a master node. The U_x and U_y displacements of the end nodes of the flanges are coupled to the chosen master node displacements U_x and U_y at the web-flange intersections. This then allows the coupling displacements U_x, U_z and R_x of all the web end nodes (including the web-flange intersection nodes) to the corresponding displacements at the chosen master node at the center of the web. Thereby end boundary conditions used in the shell model are only needed on the master node at the centroid of the web at each end of the member, see Fig. 2. Concentrated bending moments *M* are then applied at the ends of the member in the same center node, without any resulting stress concentrations. With these constraints, the end sections of the flanges and the web are allowed to “expand”, but the nodes of the flanges and web are constrained to remain on a straight line. This also allows free warping of the end sections. The end boundary conditions of both ends of the column with the described kinematic constraints are given as $U_y = U_z = R_x = 0$ at the central web node. The longitudinal displacement of the central web node at the middle of the member was also constrained to $U_x = 0$ in order to keep the central position of the beam in space.

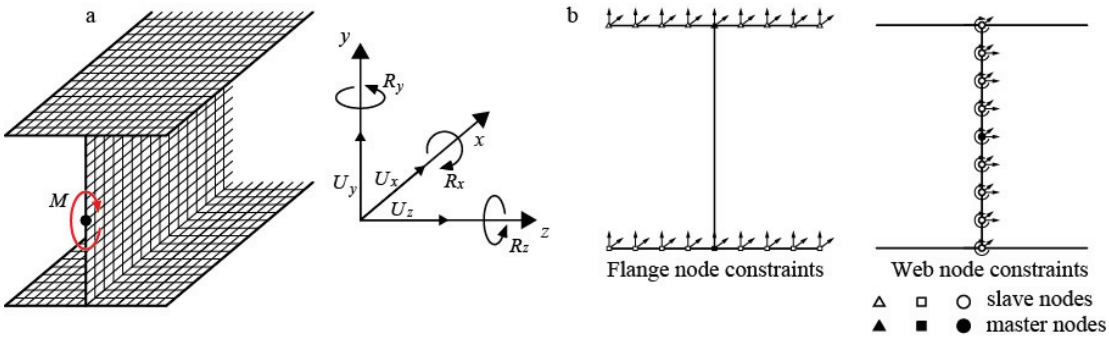

Fig. 2. Abaqus shell model (a) loading; (b) kinematic coupling constraints.

The fillet, which is not modelled has been found to have negligible influence on the LTB capacity of I profiles [6] and the mesh elements have been modelled as midline elements, leading to an unavoidable small material overlap at the web-flange junction, see Fig. 3.

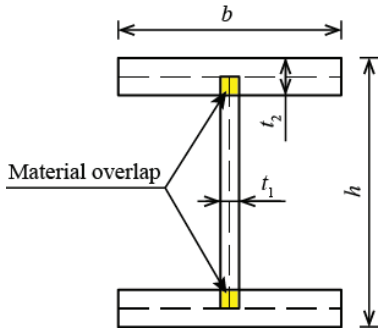

Fig. 3. material overlap in Abaqus shell model.

The imperfection of the finite element model has been included by first performing a linear buckling analysis on the perfect prismatic beam shell model with given boundary conditions under pure bending, then the relevant (displacement) normalized global buckling mode is extracted, see Fig. 4. In the following non-linear (GMNIA) finite element calculations the imperfection is established by importing the normalized displacements of the lowest global buckling mode, multiplying this by the maximal imperfection magnitudes e_0 and updating the nodal coordinates of the model by adding the established nodal imperfections.

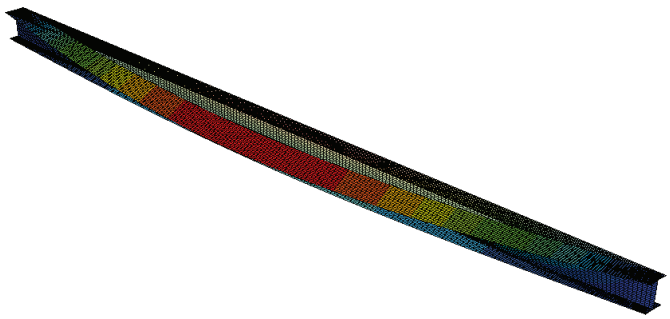

Fig. 4. Abaqus FEM shell model.

2.4. Ansys model

The commercial software program ANSYS [7] has been used for the finite element analyses using solid elements at the Czech university. The beams are modelled using the element SOLID185. It is an 8-node homogeneous structural solid element that is suitable for 3D modelling of solid structures. It has large deflection and large strain capabilities, plasticity, hyperelasticity, stress stiffening and creep. The enhanced strain formulation was considered. This formulation prevents shear locking in bending-dominated problems and volumetric locking in nearly incompressible cases. The element introduces nine internal degrees of freedom to handle shear locking, and four internal degrees of freedom to handle volumetric locking. All internal degrees of freedom are introduced automatically at the element level and condensed out during the solution phase of the analysis.

10 elements per flange width, 20 elements per web height and 2 elements per as flange as web thickness are used. Number of elements in the *x*-direction is not constant per length (non-dimensional slenderness). It was calculated in such a way that the maximal aspect ratio of the longest and shortest edges of an element does not exceed the maximal acceptable aspect ratio for quadrilaterals according to [7].

Boundary conditions are created the same way as in the Abaqus model. There are three kinematic coupling constraints on both ends of the beam: two of them are for edges of the flanges, one is for the web axis, see Fig. 5.

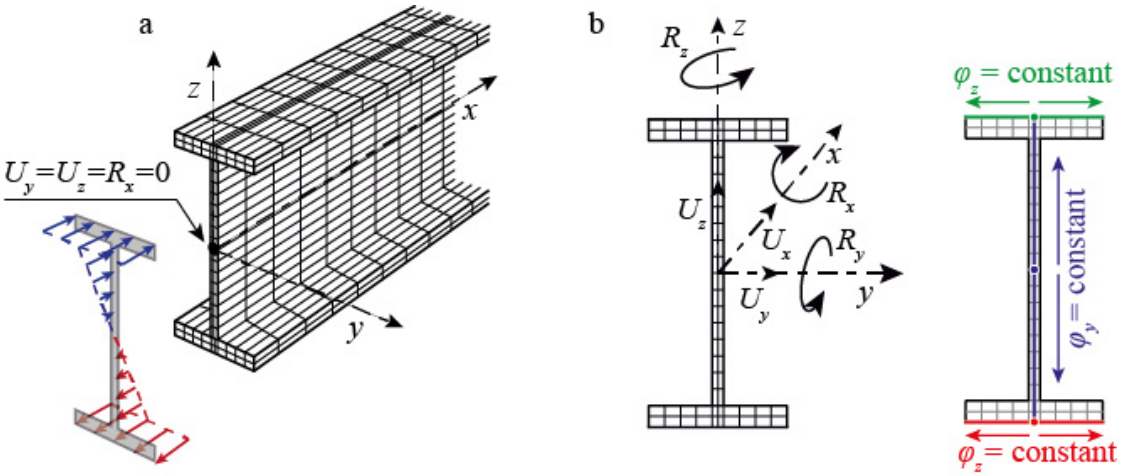

Fig. 5. Ansys solid model (a) loading; (b) kinematic coupling constraints.

The pure bending moments M on both ends are applied as a surface load in the form of pressure p. The gradient of pressure is defined by a slope value (a ratio between moment M and second moment of area I_y) and ordinate z which represents the slope direction. Thus, the magnitude of pressure is given as $p = M\,z\,/\,I_y$. The distribution of pressure is schematically illustrated in Fig. 5.

3. Random input variables

In general, the resistance M_d is a random quantity which is a function of random material and geometrical characteristics [8]. Thus, it can be studied using simulation methods, e.g. Latin Hypercube Sampling method (LHS) [9]. For this comparative analysis 10 simulation runs were generated. Material characteristics of steel grade S235 and geometrical characteristics of the cross-section IPE200 based on [8,10], and magnitude of the residual stress were the random input quantities, see Table 2. All the quantities were mutually statistically independent. The Gaussian probability distribution was considered for all quantities.

Even though the residual is stress is a very variable phenomenon [11,12,13], its mean value was considered according to [14] as 30 % of the yield stress f_y, and standard deviation as 30 % of the mean value.

Table 2. Input random variables.

Characteristic	Symbol	Mean value	Standard deviation
Cross-section height	h	200 mm	0.8847 mm
Cross-section width	b	100 mm	0.9868 mm
Web thickness	t_1	5.6 mm	0.2187 mm
Flange thickness	t_2	8.5 mm	0.3898 mm
Yield stress	f_y	297.3 MPa	16.8 MPa
Young's modulus	E	210 GPa	10 GPa
Residual stress	σ_R	89.19 MPa	26.757 MPa

4. Material model

Steel grade S235 was considered. The material model used is the one recommended in Eurocode 3 part 1-5 [15] case b). This model, which is very similar to the elastic-perfect plastic model of case a) includes a hardening slope of E/10000 in order to avoid any possible convergence issues. A more realistic hardening behavior of the material is in most cases of little importance, since the strains at the point of maximum loads are often limited in magnitude, with the positive influence of strain hardening becoming apparent only for very stocky members and in the post-buckling range.

5. Residual stress

A linear, self-equilibrating residual stress distribution is used in the FE models, included through an initial thermal loading step. The temperature change ΔT needed in a point of the cross section depends on the thermal expansion coefficient α_t (α_t = 1.2E-5 K^{-1}) and the magnitude of the residual stress σ_R to be established at that point. The temperature change needed is given as

$$\Delta T = -\frac{\sigma_R}{E\alpha_t}. \tag{3}$$

This method of residual stress introduction can only be used for true self equilibrating residual stress distributions. Since the end cross sections of the flanges and web are constrained to deform on straight lines there are no special end effects. It should be noted that the stress found in finite element analysis with low order elements are approximately constant within each element leading to a seemingly small deviation in edge stress. This should not lead to corrections.

Commonly used residual stress pattern for hot-rolled I-sections with linear stress distribution was considered for the analysis, see Fig. 6.

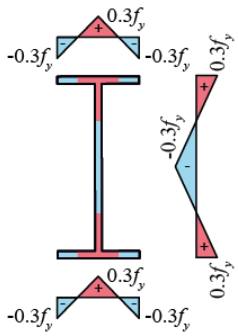

Fig. 6. linear residual stress distribution in I-shaped profiles.

6. Calculation of load-carrying capacity

When carrying out the values of load-carrying capacity in Abaqus the failure criterion used for the numerical simulations is the one recommended in Eurocode 3 part 1-5, [15], for structures susceptible to buckling, i.e. as the point at which the maximum load is attained. Thus the present analysis has been performed by employing the Static Riks (arc length method) algorithm, well known for being used in conjunction with stability problems.

In Ansys the arc length method is not used. The value of load-carrying capacity is given as a value of bending moment *M* during the last substep of calculation when the determinant of material stiffness matrix is nonzero.

7. Conclusion

A stochastic analysis of load-carrying capacity of steel beams subjected to bending was carried out. The analysis was performed in two ways: with and without considering the residual stress. The results are shown in Table 3. Mean values of load-carrying capacity of Abaqus shell models are higher than those of Ansys solid models, approximately 2-6 %. The difference in the intermediate slenderness range, where it is well-known that imperfections influence the load carrying capacity the most (due to the member failing through in-elastic buckling) is negligible. A more significant difference is in slenderness 0.3, where the difference of mean values is reaching the size close to standard deviation. This may be especially due to the pronounced plastic behavior, combined with the material overlap in the shell model, see Fig. 3, the beam being slightly stiffer [16]. The application of end moments through a linear pressure distribution in the solid model may also have a slight influence after the onset of yield. However, the crucial thing is the correlation among both models, which is almost 1 in each case. Thus, the results lie on a line, see Fig. 7. Taking into account 10 LHS runs, standard deviations of load-carrying capacity of Abaqus shell models are approximately the same as in Ansys solid models. This implies the accuracy of both approaches.

Table 3. Results.

Non-dim. slenderness $\overline{\lambda}_{LT}$ [-]	Residual stress	Ansys		Abaqus		Correlation
		Mean value [kNm]	St. deviation [kNm]	Mean value [kNm]	St. deviation [kNm]	
0.3	*with*	56.819	3.724	60.166	3.848	0.996
0.3	*without*	56.976	3.755	60.230	3.828	0.999
0.6	*with*	49.348	2.669	51.210	2.854	0.999
0.6	*without*	52.645	3.210	54.076	3.289	1.000
1.2	*with*	27.862	1.820	28.545	1.932	0.999
1.2	*without*	29.791	2.008	30.459	2.128	0.999

Even though it is common to model LTB problems using shell elements instead of solid elements, there are some undesirable effects associated with shell elements, e.g. the material overlap at the web-flange junction. However, this issue can be eliminated by the introduction of beam elements along the length of the member, at the web-flange junctions, through which the fillet radius is also modelled, see [17]. Another disadvantage of using shell elements is a problematic modelling of varying thickness of a cross-section, while solid elements eliminate these effects. A specific instance where solid elements are more appropriate is the modelling of members in which the variation of residual stresses through plate thickness is non-negligible, while shell elements should be used for slenderer sections for which local imperfections affect the load carrying capacity. Both approaches allow the modelling of the effects of residual stresses that cannot be taken into account in the close-form analytical solution [18]. However, it is done at the cost of increasing the CPU time.

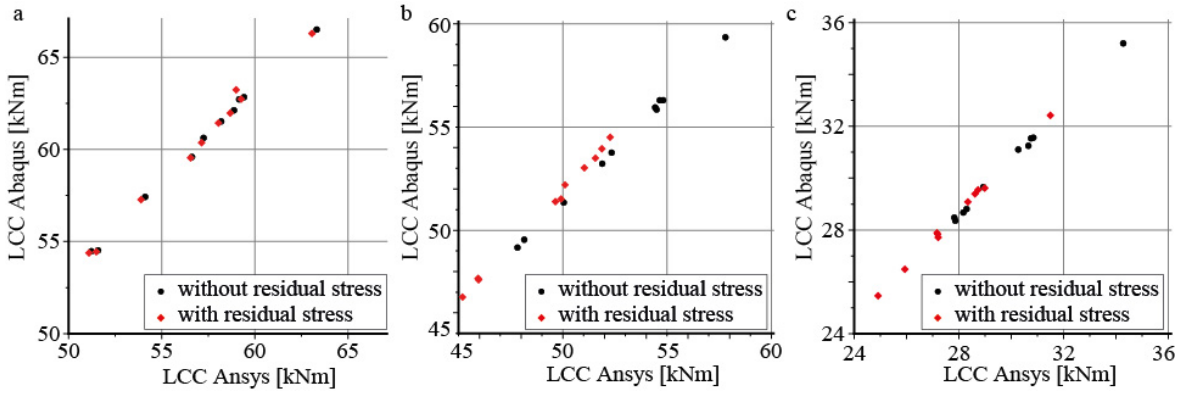

Fig. 7. Graphs of load-carrying capacity for slenderness (a) 0.3; (b) 0.6; (c) 1.2.

Acknowledgements

The work has been supported by the grant project GAČR 14-17997S.

References

[1] N. Boissonnade and H. Somja, Influence of Imperfections in FEM Modelling of Lateral Torsional Buckling, Proc. Annu. Stab. Conf., pp. 1–15, 2012.
[2] R. Maquoi and J. Rondal, Mise en equation des nouvelles courbes Européennes de flambement, Construction Métallique, vol. 1. pp. 17–29, 1978.
[3] N.S. Trahair, The Behaviour and Design of Steel Structures, John Wiley and Sons, Ltd., 1977.
[4] EN 1993-1-1:2005 (E): Eurocode 3: design of steel structures—part 1–1: general rules and rules for buildings, CEN; 2005.
[5] ABAQUS CAE, v6.13-4, Simulia, 2014.
[6] P. Kaim, Spatial buckling behaviour of steel members under bending and compression, PhD Thesis, Graz University of Technology, Austria, 2004.
[7] ANSYS, Inc.: Release 12.1 Documentation for ANSYS. SAS IP, Inc 2010.
[8] J. Melcher, Z. Kala, M. Holický, M. Fajkus, L. Rozlívka, Design characteristics of structural steels based on statistical analysis of metallurgical products, Journal of Construction Research 2004; 60(3-5): pp. 795–808.
[9] M.D. McKey, W.J. Conover, R.J. Beckman, A Comparison of Three Methods for Selecting Values of Input Variables in the Analysis of Output from a Computer Code, Technometrics, Vol. 21, No. 2, pp. 239-245, 1979.
[10] Z. Kala, J. Melcher, L. Puklický, Material and geometrical characteristics of structural steels based on statistical analysis of metallurgical products, Journal of Civil Engineering and Management 2009; 15(3):299–307.
[11] I. Daddi, F. M. Mazzolani, Détermination expérimentale des imperfections structurales des profilés en acier, Construction métallique, n. 1, 1974, pp. 24–45.
[12] S. Shayan, K.J.R. Rasmussen, H. Zhang, Probabilistic modelling of residual stress in advanced analysis of steel structures, Journal of Constructional Steel Research 101 (2014): pp. 407–414.
[13] H. Zhang, S. Shayan, K. J. R. Rasmussen, B. R. Ellingwood, System-based design of planar steel frames, I: Reliability framework, Journal of Constructional Steel Research 123 (2016): pp. 135–143.
[14] European Convention For Constructional Steelwork, Ultimate Limit State Calculations of Sway Frames with Rigid Joints - No. 33, 1984.
[15] EN 1993-1-5:2006. Eurocode 3: Design of steel structures – Part 1.5: Plated structural elements, CEN - European committee for Standardization, Brussels (Belgium), 2006.
[16] J. Jönsson, T. C. Stan, European column buckling curves and finite element modelling including high strength steels, Journal of Constructional Steel Research, (*in review*)
[17] Greiner R, Kettler Ms, Lechner A, Freytag B, Linder J, Jaspart J-P, Boissonnade N, Bortolotti E, Weynand K, Ziller C, Oerder R. SEMI-COMP: Plastic member capacity of semi-compact steel sections - a more economic design, European Commission, Research Fund for Coal and Steel, Luxembourg: Office for Official Publications of the European Communities, 2009, doi: 10.2777/54746
[18] Z. Kala, Sensitivity and reliability analyses of lateral-torsional buckling resistance of steel beams, Archives of Civil and Mechanical Engineering 2015; 15(4): pp. 1098–1107.